Escola de Primavera de Transição e Turbulência
Blumenau 2020

ABCM Associação Brasileira de Engenharia e Ciências Mecânicas

12th Spring School on Transition and Turbulence
September 21st-25th, 2020, Blumenau, SC, Brazil

EPTT-2020-0023
EMPIRICAL AERODYNAMICS OF BIO-INSPIRED WINGS

Guilherme J. A. Pimentel
Instituto Tecnológico de Aeronáutica – ITA, Praça Marechal Eduardo Gomes, 50 - Vila das Acacias, São José dos Campos.
pimentelgjap@ita.br

Heidi Korzenowski
Universidade do Vale do Paraíba – UNIVAP, Av. Shishima Hifumi, 2911 - Urbanova, São José dos Campos.
heidi@univap.br

Abstract. *This work aims to present to the scientific community an experimental aerodynamic analysis on the biomimetization of three-dimensional wings, whose analysis is part of the author's Undergraduate Thesis. In this paper, the aerodynamic behavior of two sets of NACA 2412 and Clark Y airfoils with wavy leading-edge, biomimetized from the humpback whale fins, will be presented. Wavy leading edges have been investigated as a flow control mechanism and perform better in drag reduction caused by the delay in the detachment of the boundary layer, increasing the stall angle and consequently increasing the maximum lift coefficient (C_{lmax}). Forces measurements were performed for a better understanding of the phenomenology involved. Force measurements indicate that the NACA 2412 profile responded positively to the biomimetization. Therefore, it is evident in these experiments that the biomimetization benefited the performance when causing the delay of the boundary layer detachment, increasing the lift and the stall angle and decreasing the drag generation. However, the Clark Y profile did not respond as expected. The drag values were higher and lift values were lower compared to its smooth model. However, the stall of the models always decreased smoothly, without an abrupt drop of lift.*

Keywords: *Biomimicry; Aerodynamics; Wavy leading-edge; Airfoils*

1. INTRODUCTION

1.1. Biomimicry

Biomimicry is the science that, from the observation of organisms and forms of nature and the understanding of how they adapt to certain situations and become distinct and unique in their midst. Then, it applies this knowledge in various designs applied to human life, extending to areas such as engineering, medicine, architecture and fashion, among others (Gad-El-Hak, 2000). In engineering, biomimicry is used to pursue solutions to problems related to consumption, mechanical stress, and design, among others. Thus, using nature as a source of inspiration and innovation. In Japan, for example, the Shinkansen JR700 bullet train could reach speeds up to 300 km/h, but its noise exceeded the environmental standards of sound pollution. Then, the design of the front side of the train was redesigned, inspired by the Kingfisher Bird, allowing the trips to be quieter but also 10% faster and 15% more economical (Spaho, 2011).

1.1. Flow control

Flow control devices have been widely studied over the years. The motivation for this study involves a potential gain in hydrodynamics and aerodynamics performance in engineering design such as wings, control surfaces, propellers, turbines, automotive airfoils, etc. The wavy leading edge has been investigated as a flow control mechanism that performs better in the drag reduction caused by the delay in the detachment of the boundary layer, increasing the stall angle and consequently increasing the maximum lift coefficient when compared with smooth leading edges. In this sense, it is necessary to analyze the phenomenology of bio-inspired wings aerodynamics, performing aerodynamic forces measurements and flow visualizations in wind tunnel on wings with wavy leading edge (Miklosovic, 2007a).

Flow changes may cause simultaneous benefits. The flow control mechanism delays the laminar-turbulent transition and maintains the laminar boundary layer on the back of the airfoil, decreasing shear stress and vortex generation. Also, some effects caused by flow control mechanisms can improve performance in some parts, but at the same time worsen others. Since lift control, drag and aerodynamic efficiency are the main development objectives in aeronautical engineering, understanding the typical flow control mechanisms to increase lift and decrease drag is essential to obtain the possible benefits of the wavy leading edge as flow controls in aeronautical engineering (Skillen, 2014).

In 2004, a study was conducted to understand the morphology of the humpback whales' fin and verify its performance. After wind tunnel measurements, it was found that the fins with such tubercles offered a delay in the stall angle of 40%, when compared with smooth-edged fins, while the lift was increased, and the drag was decreased. These improvements are possible because these structures act as vortex generators, which maintain the lift force and prevent stalling at high angles of attack (Miklosovic, *et al*., 2004 b). The tubercles' flow control might be associated with the ability of humpback whales to perform rapid rotating maneuvers with a lower radius and maintain high lift values at high angles of attack (Fish, 1995).

1.2. Biomimicry applied to flow control mechanisms

A study of the effect of wavy leading-edge on two-dimensional and three-dimensional flows was carried out. A NACA 0020 airfoil was performed in a wind tunnel for a Reynolds number range between 274,000 and 277,000. When the wavy and smooth airfoils were compared, it was observed that the stall behavior is more gradual and takes longer to occur in the wavy model (Miklosovic, 2007a).

These tubercles modify the pressure distribution along the wingspan, different numbers of critical Mach may also occur in some regions. Some areas may have a higher number of critical Mach than other areas when compared to a smooth leading-edge. This critical Mach number variation along the wingspan can lead to lower growth of the drag force associated with the critical Mach number (Johari, 2007).

In pre-stall conditions, infinite wings and finite wavy wings models show similar behavior. At high stall angles, the infinite wing shows a significant aerodynamic decay with substantial losses in its maximum lift, as shown in Fig. 1 below:

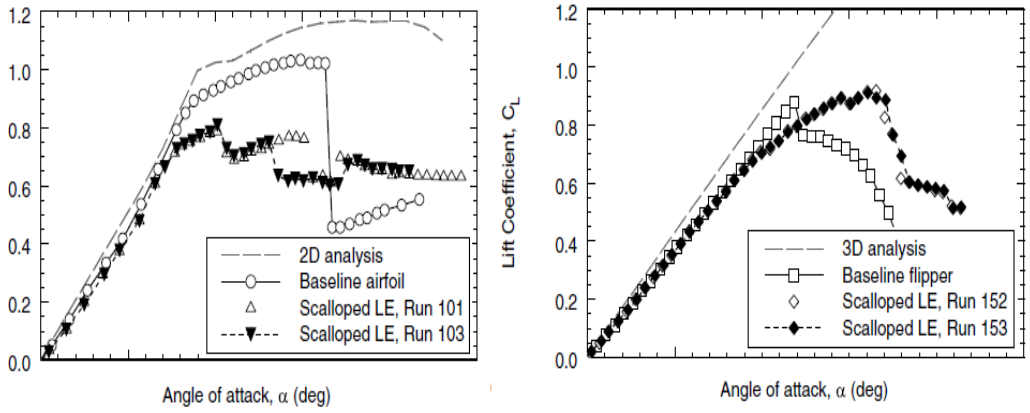

Figure 1. Effects of the wavy leading-edge.

The benefits of the aerodynamic and hydrodynamic characteristics of the post-stall wavy configuration are in the delay of the stall condition and a smooth stall behavior and, in some cases, tubercles increase lift performance (. Therefore, it seems appropriate to biomimic the pectoral fins of the Humpback whale to improve the performance of the control surfaces of engineering systems such as boat rudders, missile and torpedo fins, horizontal aircraft stabilizers, ailerons, wind turbine blades, etc. (Bolzon, 2014)

This work aims to present an experimental aerodynamic analysis on the biomimetization of three-dimensional wings, whose analysis is part of the author's Undergraduate Thesis. The aerodynamic behavior between two sets of wings with different airfoils shape, NACA 2412 and Clark Y, with wavy leading-edge, bio-inspired from the humpback whale fins will be presented and compared. Forces measurements were carried out and flow visualization experiments were performed using wool tufts for a better understanding of the phenomenology involved and to analyze regions of boundary layer detachment, vortex generation and compare the performance, related to lift and drag.

2. METHODOLOGY

2.1. Wings design

To investigate the effects of the wavy leading-edge, two sets of three models were prototyped. Each set consists in a Baseline model (X-BL) and two wavy models (X- γ- λ), where X is represented by the initials of the airfoil used ("N" for NACA 2412 and "C" for Clark Y), with a constant chord size (c) and different amplitudes (γ) and wavelength (λ) defined by a percentage of the chord, following the characteristics detailed in Tab. 1 below:

Table 1. Geometrical characteristics of the wing models.

Airfoil	Amplitude (γ)	Wavelength (λ)	Configuration
Clark Y	0% c	0% c	CBL
Clark Y	3% c	11% c	C3γ11λ
Clark Y	6% c	22% c	C6γ22λ
NACA2412	0% c	0% c	NBL
NACA2412	3% c	11% c	N3γ11λ
NACA2412	6% c	22% c	N6γ22λ

The airfoils (Figs. 2 and 3) were designed using the CAD (Computer-Aided Design) software Autodesk Inventor®. The wavy leading edges were designed based on a two-dimensional airfoil with different chord sizes. These airfoils were combined on the leading-edge following a sinusoidal guide defined by a wavy geometry. Each airfoil had 150 cm of chord and a wingspan size of 37 cm (NACA 2412) and 33.4 cm (Clark Y).

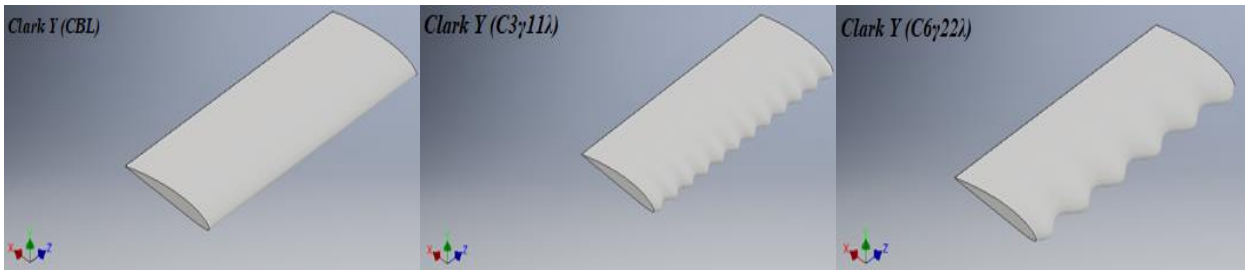

Figure 2. CAD of the Clark Y models.

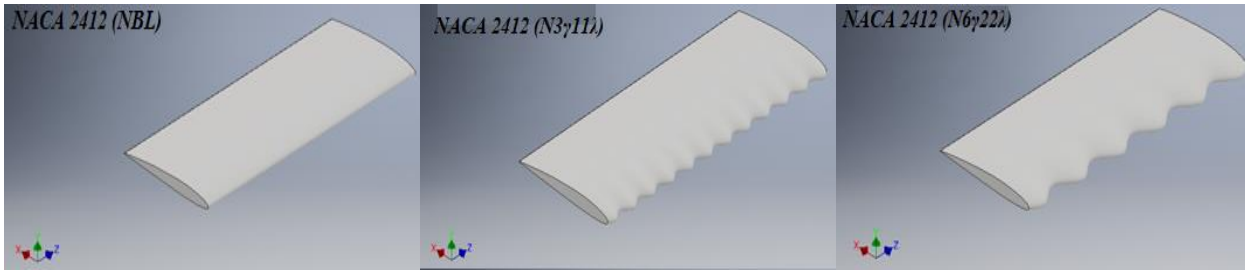

Figure 3. CAD of the NACA 2412 models.

After the design project, the models were then prototyped with PLA (Polylactic Acid) in a 3D-Printer, as shown in the Figs. 4 and 5 below:

Figure 4. Clark Y models prototyped.

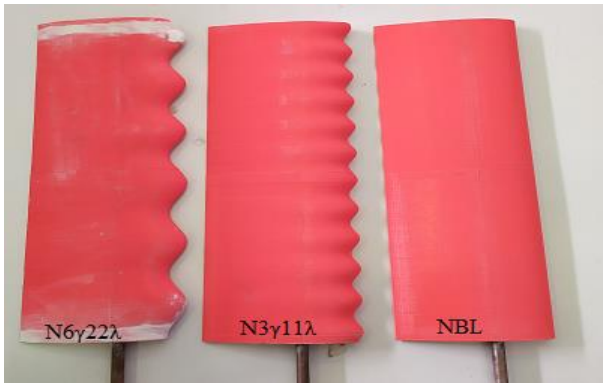

Figure 5. NACA 2412 models prototyped.

2.2. Wind tunnel

The experiment was conducted at the Professor Kwei Lien Feng Laboratory subsonic wind tunnel. This open return wind tunnel has a test section with 457mm x 457mm x 1200mm of dimension, with a velocity of 23 m/s and Re = 215.000. The aerodynamics forces were acquired using a cell load, which was calibrated in every change of airfoil, that converts the load received by the wings in intensity of electric signs, which is interpreted by the software LabView®. The same software provides the data of lift, drag and moment curves.

2.3. Loads measurements

As mentioned before, two sets of prototyped wings were used in the experiments. Each set has its own airfoil model (Clark Y and NACA 2412) but the same wave equation configuration. These airfoils were selected because of their high range of previous studies and works, so, the wavy airfoils' performance can be easily compared later. The first set performed was the Clark Y airfoils, beginning with the Baseline model, followed by the $3\gamma 11\lambda$ model and then, the $6\gamma 22\lambda$ model.

The angle of attack was varied between -4° and 30° along with the experiment. Each time that the angle was changed, in intervals of 2° each, the LabView® software registered and plotted the respective values of lift and drag load for each angle. To avoid possible imprecisions at the data acquirement, each experiment was performed three times for long (Repeatability Method). The local temperature and pressure on that day were 71,6° F and 954,00 mbars.

2.4. Flow visualization

The objective of the flow visualization was to observe the detachment of the boundary layer (regions and detachment directions) and regions of vortex generation and recirculation. For that, the flow visualization with wool tufts was used. Columns of wool tufts were fixed along the surface of each model and its color was chosen to be contrasted with the wing surface color so that it can be easier to observe the flow.

Photos were taken at certain angles of attack (0º, 14º and 20° for Clark Y and 0°, 12° and 15° for NACA 2412), in function of the stall angle defined by the lift plots. Details of the arrangement of the filaments on the Clark Y and NACA 2412 airfoils are shown in Figs. 7 and 8.

Figure 6. Wool tufts on the Clark Y upper surface.

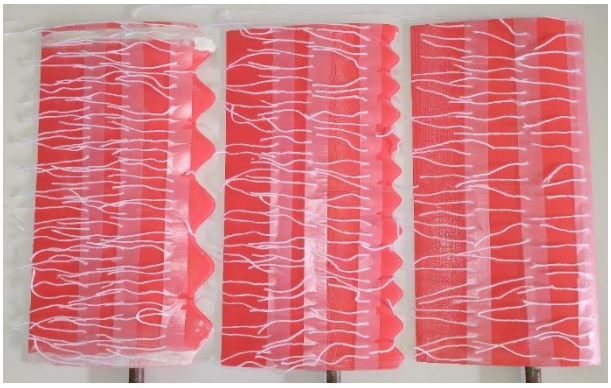

Figure 7. Wool tufts on the NACA 2412 upper surface.

3. RESULTS AND DISCUSSION

In this section we'll analyze the aerodynamics forces plots and discuss the flow behavior, observing and identifying the boundary layer detachment. The final performance analysis is summarized in Tab. 2 below and the detailed and discussed information of each set are in the following subsections.

Table 2. Comparisons of final values among models.

Model	Stall angle (°)	Lift (N)	Drag (N)	Lift gain (%)	Drag gain (%)
CBL	18	1,263	0,542	-	-
C3γ11λ	16	1,261	0,58	-0,16	+7,01
C6γ22λ	16	1,199	0,606	-5,06	+11,8
NBL	14	1,125	0,749	-	-
N3γ11λ	16	1,165	0,692	+3,55	-7,61
N6γ22λ	20	1,175	0,653	+4,44	-12,81

3.1. Clark Y analysis

The first observation made after plotting the lift and drag graphs is that the stall angle of the CLB was greater than that described in the literature. The Aerodynamic Forces vs. α chart are shown in Figure 8:

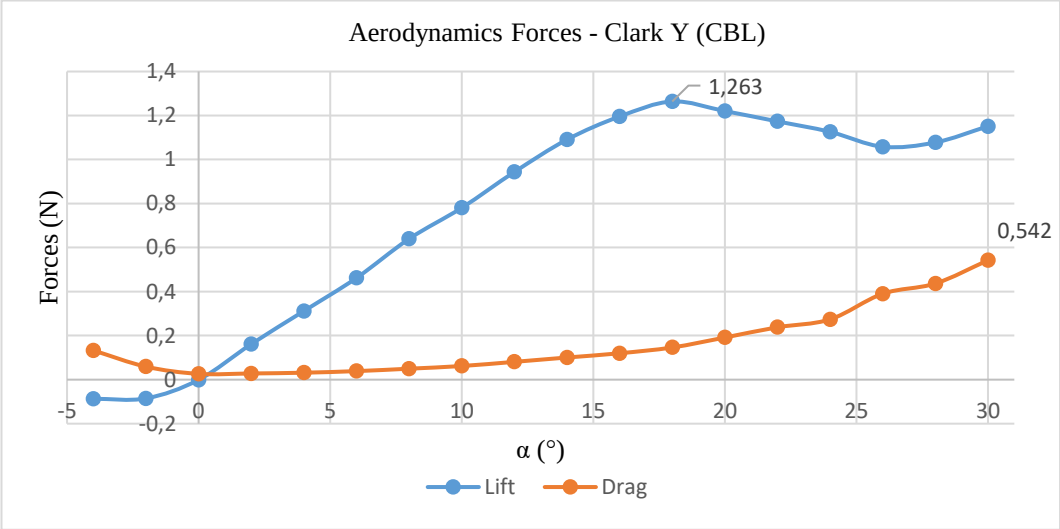

Figure 8. Lift and Drag Curve vs. α (CBL)

We can observe that the maximum pre-stall angle is 18° and indicates a lift value of 1,263 N. The stall is not abrupt, and the lift decreases smoothly as the α increases while the drag force is amplified parabolically. In Figs. 9, 10 and 11 below, the wool tufts indicate the presence of wingtip vortex and show the phases of the boundary layer detachment. In Figure 10, we can observe that the detachment of the boundary layer starts from the root of the wing and expands towards the wingtip. In Figure 11, the boundary layer is totally detached from the post-stall angle with indications of recirculation regions.

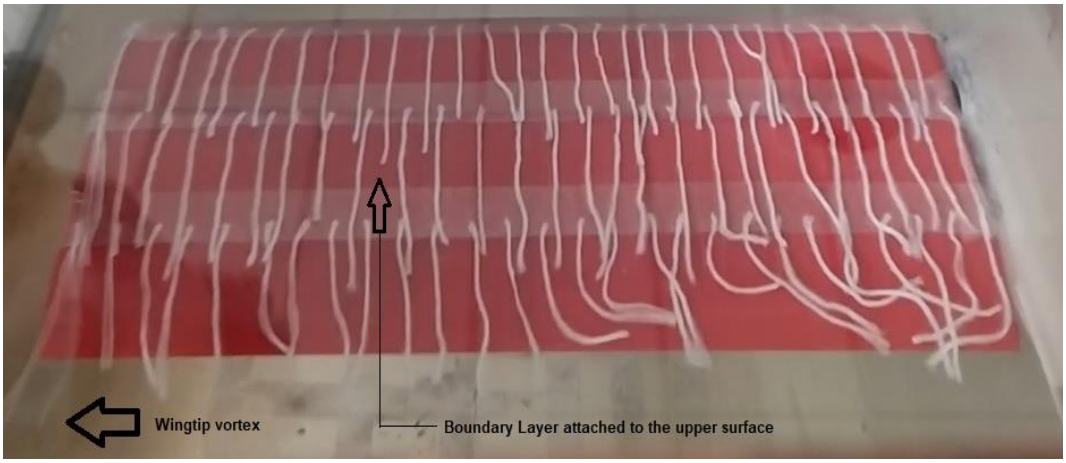

Figure 9. Wingtip vortex and boundary layer attached to the upper surface. Clark Y (CBL) at α= 0°

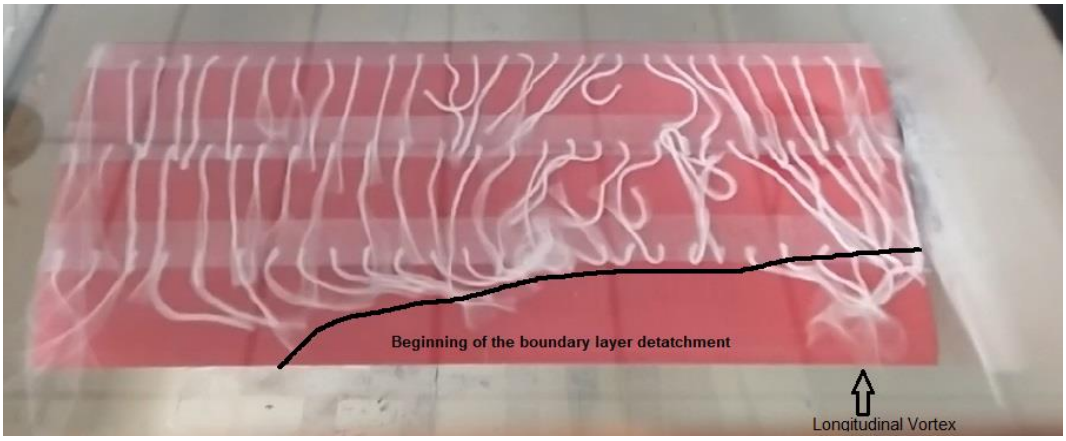

Figure 10. Beginning of the flow separation and longitudinal vortex. Clark Y (CBL) at α= 14°

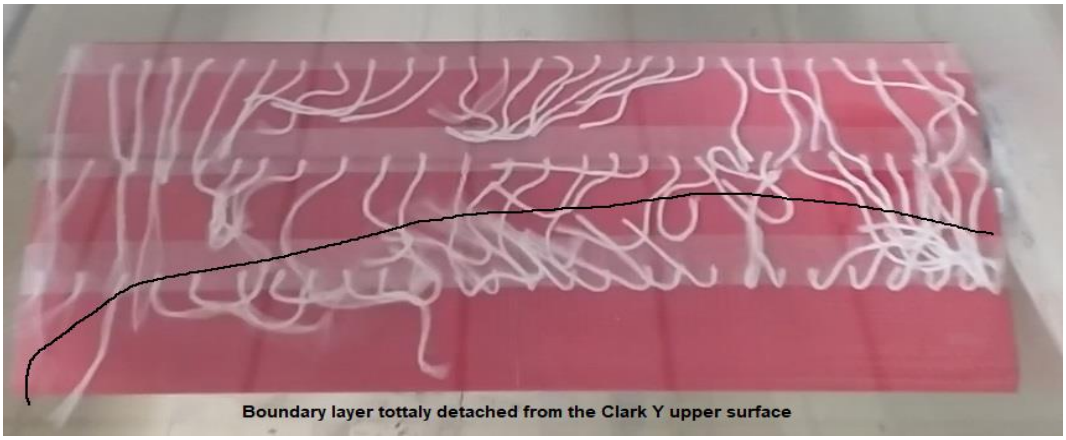

Figure 11. Flow totally separated. Clark Y (CBL) surface at α= 20°

The stall angle of the model C3γ11λ is the same as described in the literature, with the total boundary layer detachment at α nearly 16º. However, the decay of the lift was even smoother than the CBL configuration. The post-stall occurred almost linearly, indicating that this wavy configuration can maintain a considerable lift force at high α. In addition to a smaller stall angle, this configuration showed an increase of drag when compared to the CBL configuration. Therefore, this analysis indicates that the C3γ11λ model does not perform well to the biomimicry, considering that the lift in a critical α is lower and that the drag is higher. In Fig. 12 below we can analyze the plots of aerodynamic forces in function of α and analyze their characteristics:

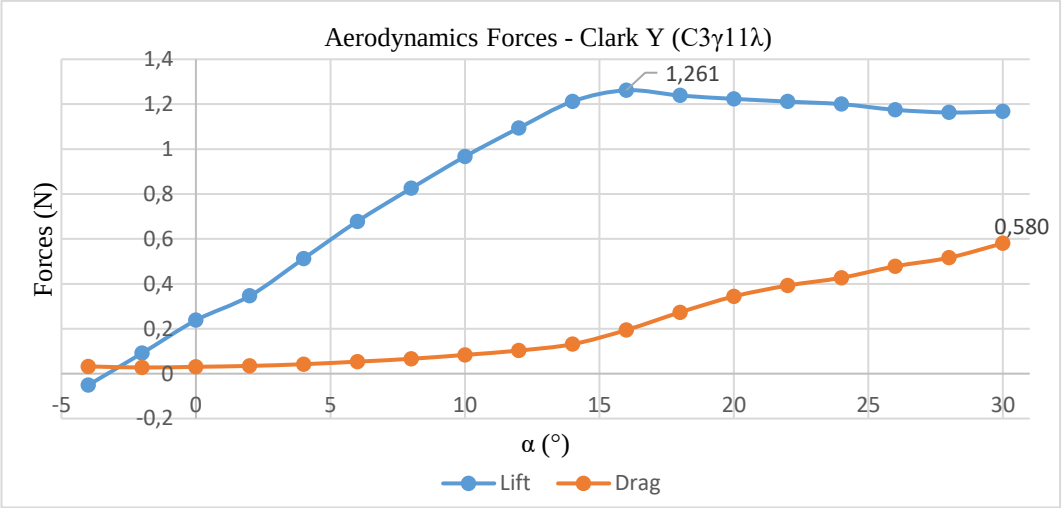

Figure 12. Lift and Drag Curve vs. α (C3γ11λ)

In the boundary layer detachment phases, Figs. 13 and 14, it is observed that the detachment area of the boundary layer is larger and, therefore, explaining why the C3γ11λ configuration has a smaller stall angle. It is also possible to notice a more intense recirculation region near the wind tunnel wall:

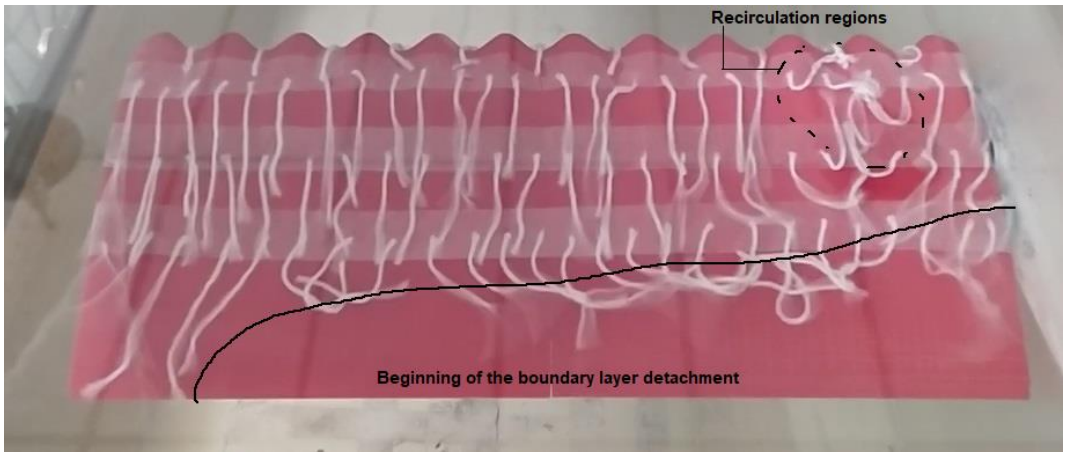

Figure 13. Beginning of the flow detachment and recirculation regions. Clark Y (C3γ11λ) at α= 14°

Figure 14. Flow totally perturbed. Clark Y (C3γ11λ) at α= 20°

The model C6γ22λ also presented stall at α= 16°, but with a value even lower than the model C3γ11λ, as observed in Fig. 15 below:

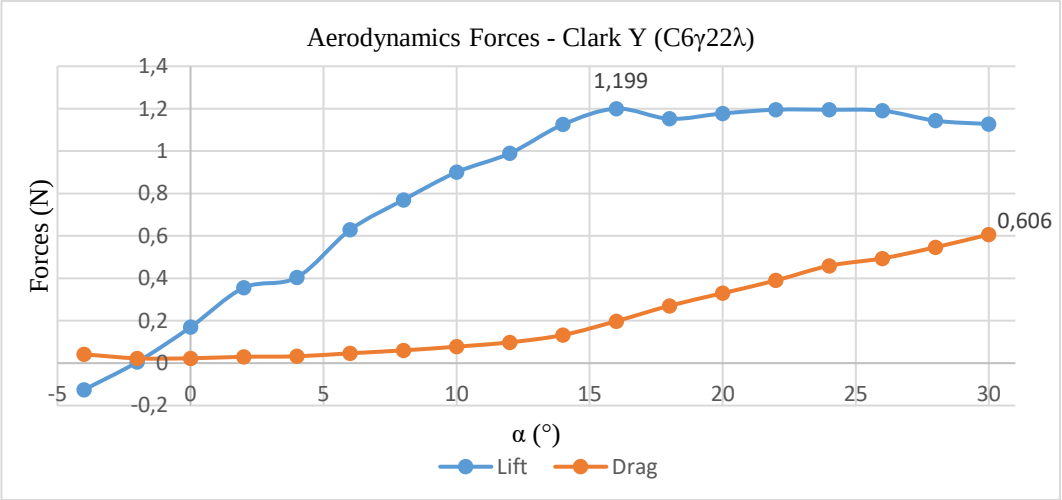

Figure 15. Lift and Drag Curve vs. α (C6γ22λ)

The maximum lift value reached was 1.199 N, with a final drag force of 0.606 N. There was no aerodynamic improvement, although the post-stall behavior was similar to the previous one. The phases of boundary layer detachment are shown in Figs. 16, 17, and 18 below:

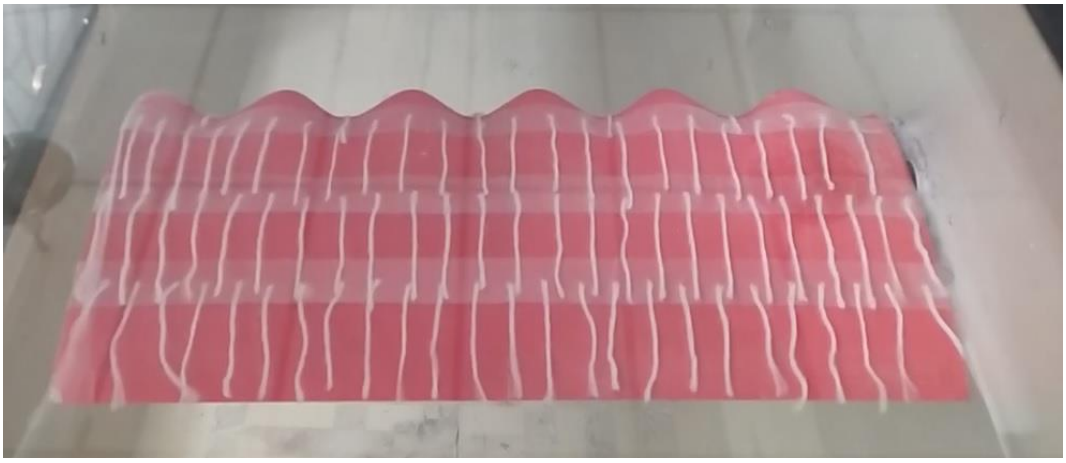

Figure 16. Flow attached to the surface. Clark Y (C6γ22λ) at α= 0°

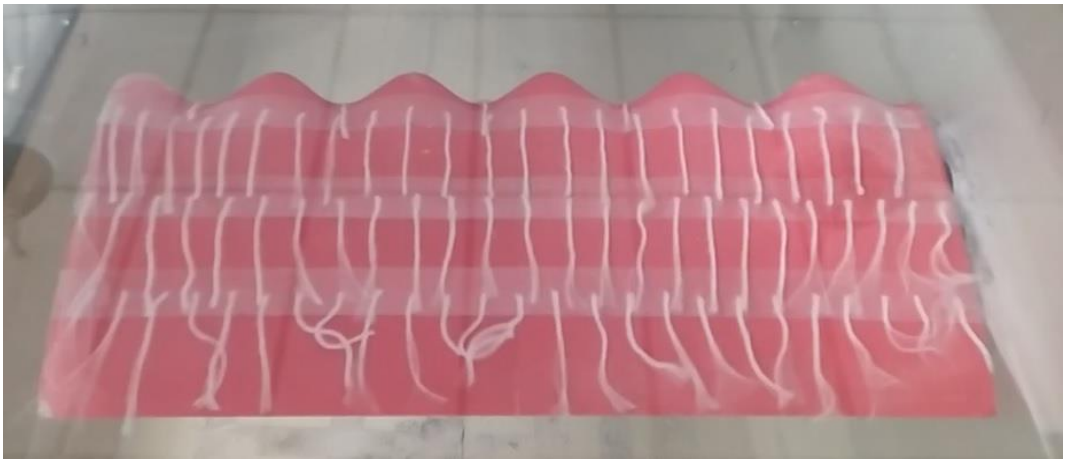

Figure 17. A soft detachment of the flow. Clark Y (C6γ22λ) at α= 14°

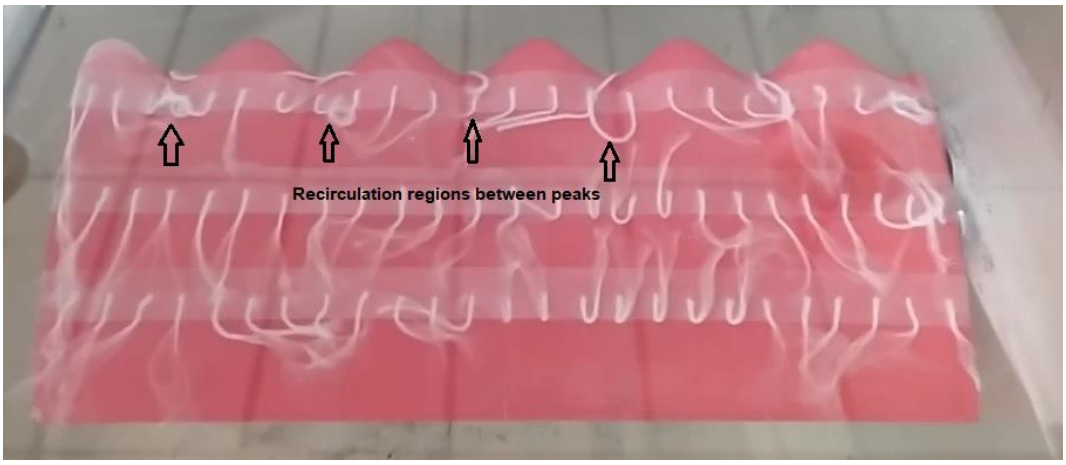

Figure 18. Recirculation regions between peaks of the wavy leading edge. Clark Y (C6γ22λ) at α= 20°

When α= 14°, the flow seems to be less disturbed compared to the previous model at the same angle of attack: At α= 20°, the boundary layer is already fully detached.

3.2. NACA 2412 analysis

After the wind tunnel experiments with the smooth (NBL) and wavy (N3γ11λ and N6γ22λ) models, the plots data were treated and analyzed to identify some type of abnormality and lack of consistency. In the end, we obtained the lift and drag curves shown in Figs. 19, 23 and 25.

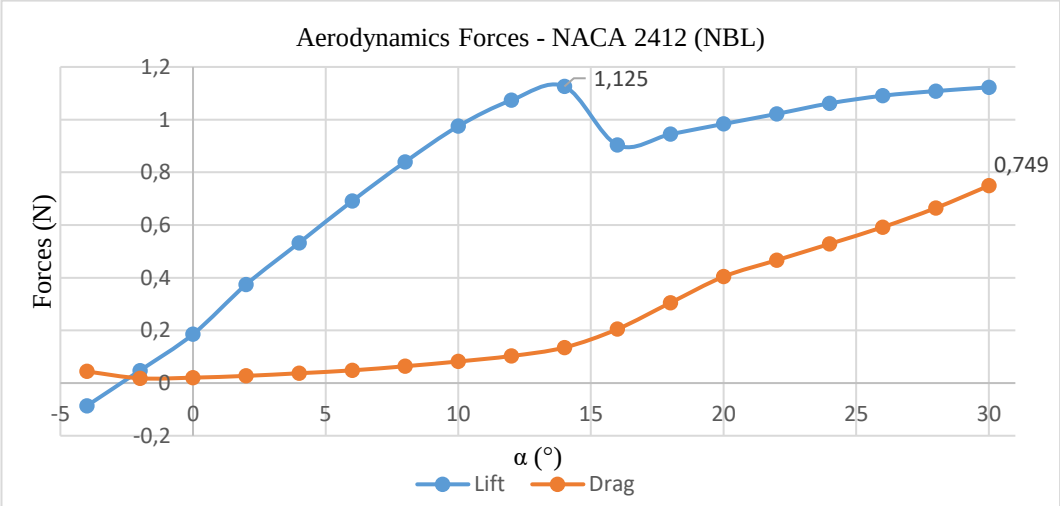

Figure 19. Lift and Drag Curve vs. α (NBL)

The first observation made after plotting the force graphs was about the stall angle of the NBL model. The maximum α was at 14°, presenting a lift value of approximately 1.25 N. The drag force intensifies as α increases, reaching a value of 0.749 N. In Fig. 20, we can observe the boundary layer totally attached on the upper surface of the wing:

Figure 20. NACA 2412 at α= 0°

In Fig. 21, the boundary layer is close to detach (α= 12°). It is possible to notice the beginning of the flow degradation at the root runoff to the wingtip. In Fig. 22, when α= 15°, the boundary layer is almost completely causing a stall, as indicated at the lift curve for this model:

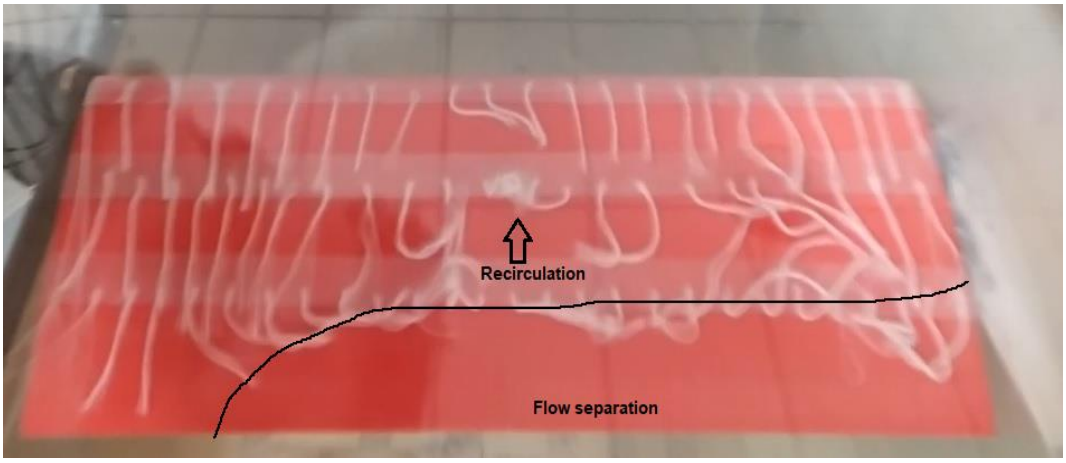

Figure 21. Beginning of the flow separation and a recirculation region. NACA 2412 at α= 12°

Figure 22. Flow totally separated. NACA 2412 at α= 15°

Analyzing the graph of the wavy model N3γ11λ (Fig. 23), it is observed that the stall happens when α= 16° approximately and occurs less abruptly, indicating a maximum value of 1.165 N. In addition to the increase of the stall angle (from 14° to 16°), the maximum lift value reached was 3.55% higher when compared to the smooth NBL model.

The drag force followed a smoother increasing behavior reaching a final value of 0.692 N, 7.61% lower than the drag of the smooth model.

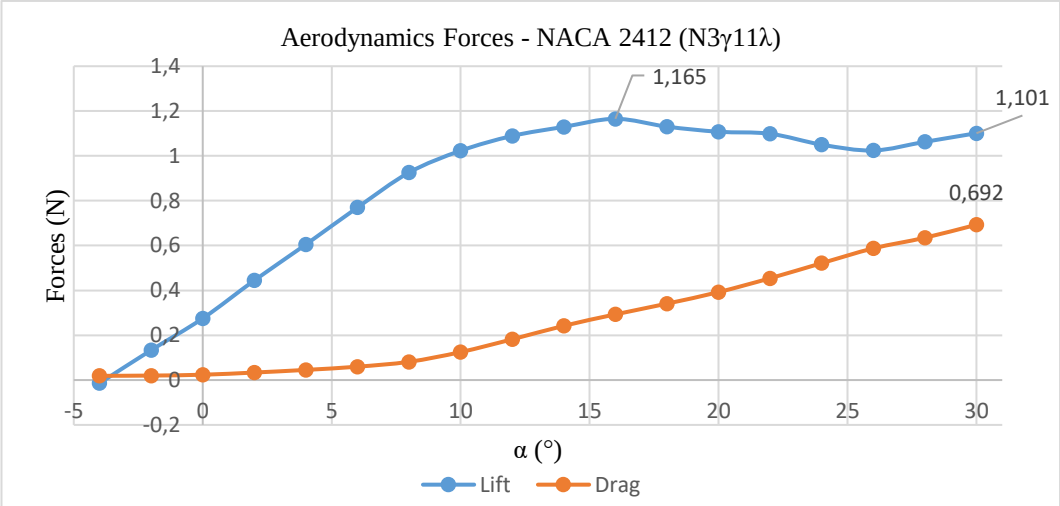

Figure 23. Lift and Drag Curve vs. α (N3γ11λ)

In α= 12°, Fig. 24, the detachment seems to be starting at the central region of the upper surface. Recirculation regions are also more intense in this section:

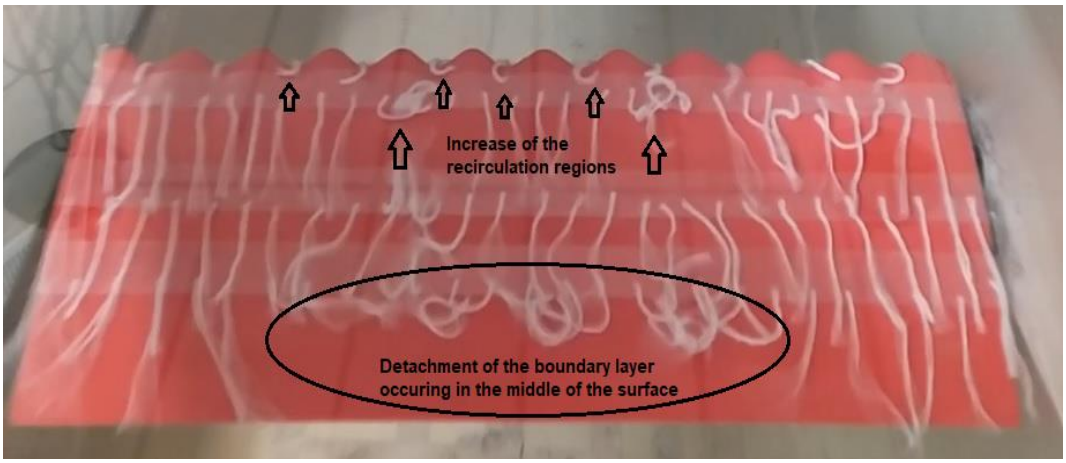

Figure 24. The detachment of the boundary layer in the middle of the surface and recirculation regions. NACA (N3γ11λ) at α= 12°

In the N6γ22λ model, the stall occurs even softly with an almost linear post-stall behavior. The maximum lift value reached before the stall was 1.175 N (0.86% higher than the N3γ11λ model) in α= 20°, which is a significant increase. The drag had behavior like the previous one and with a value of 0.653 N, which is lower than the others. These data can be observed in the lift and drag curves in Fig. 25 below:

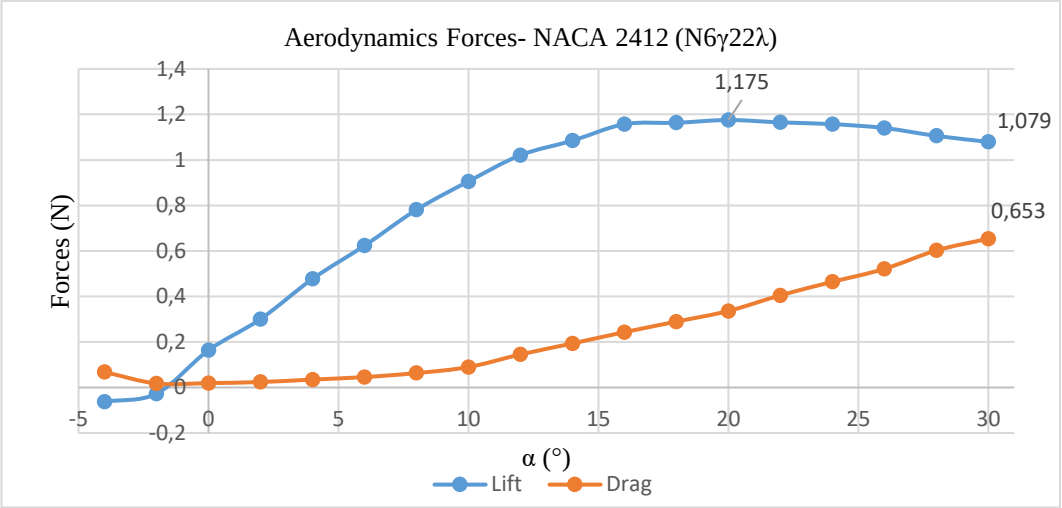

Figure 25. Lift and Drag Curve vs. α (N6γ22λ)

The flow visualization experiments indicate that the detachment phases of model N6γ22λ obtained a behavior like the N3γ11λ model. These phases are shown in Figs. 26, 27, and 28. When in α= 12° (Fig. 27), the detachment also seems to start in the central region of the upper face, being more intense near the leading edge. The recirculation region has a greater amplitude when compared with the other models. In α= 15 (Fig. 28), we can observe an almost total detachment of the boundary layer:

Figure 26. NACA 2412 (N6γ22λ) at α= 0°

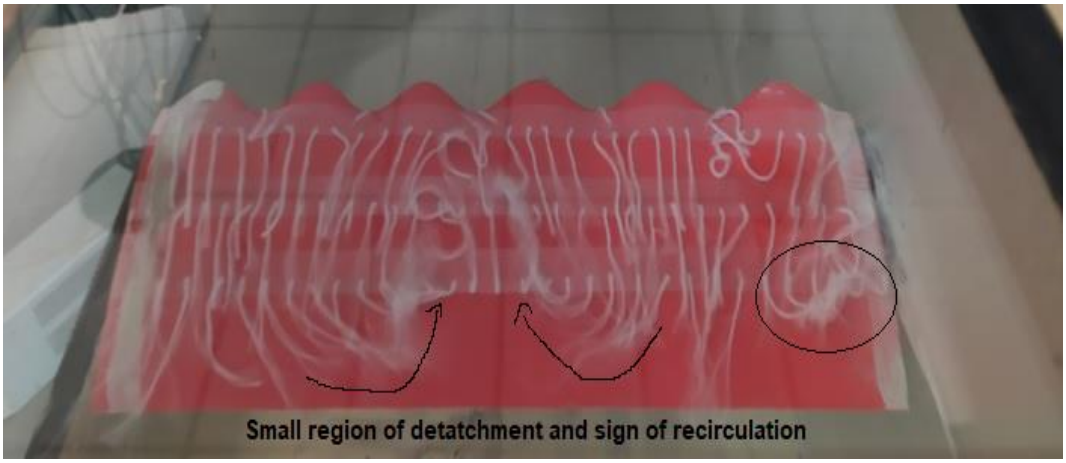

Figure 27. Smaller region of flow detachment and signs of recirculation. NACA 2412 (N6γ22λ) at α= 12°

Figure 28. Stall of NACA 2412 (N6γ22λ) at α= 15°

4. CONCLUSIONS

Force measurements indicate that the NACA 2412 profile responded positively to biomimetization. The best configuration that showed a better increase in stall angle, high gain of lift, and a better drag decrease was the model N6γ22λ. There is also a performance improvement in the N3γ11λ configuration. Therefore, it is evident in these experiments that biomimetics increased the performance to delay the detachment of the boundary layer, increasing the stall angle. However, the Clark Y airfoil did not respond as expected. The drag values were higher, and lift forces were lower compared to its smooth model (CBL). However, the stall of the models always occurred smoothly, without an abrupt drop of lift. This observation shows what has already been observed in Miklosovic's experiments, where it is said that the effect of the wavy leading-edge depends on the geometric shape and the turbulence regime in which it is immersed. Further investigations will be conducted to understand how exactly the wavy leading-edge phenomena works and if this can be applied in other designs.

5. ACKNOWLEDGMENTS

I would like to say to thank you to Prof. Dr. Adson Agrico, from ITA's Aircraft Design Department, for opening the doors of his research group, to my research colleague Paulo Henrique for helping me in the execution of the experiments and to the entire technical team of Feng's Wind Tunnel Laboratory that was very important for the execution of the experiments.

6. REFERENCES

Bolzon, M. D; Kelso, R. M.; Arjomandi, M. *The effects of tubercles on swept-wing performance at low angles of attack*. 19th Australasian Fluid Mechanics Conference. Melbourne, Australia. Conference Paper: pp. 8-11, 2014.

Fish, F. E; Battle, J. M. *Hydrodynamic design of the humpback whale flipper*. Journal of Morphology, v. 225, p. 51-60, 1995.

Gad-El-Hak, M. *Flow Control: Passive, Active, and Reactive Flow Management*, first edition. New York, Cambridge University Press, 2000.

Hansen K, L.; Kelso R, M.; Dally B, B. *An investigation of three-dimensional effects on the performance of tubercles at low Reynolds number*. Proceedings of the 17th Australasian Fluid Mechanics Conference. Auckland, New Zealand, 2010.

Johari, H.; Henoch, C.; Custodio, D.; Levshin, A. *Effects of leading-edge protuberances on airfoil performance*. AIAA J 45:2634–42. 2007.

Miklosovic, D.S.; Murray, M.M.; Howle, L.E. *Experimental evaluation of sinusoidal leading edges*, Journal of Aircraft, Vol. 44, No. 4, pp. 1404-1407, 2007.

Miklosovic, D.S.; Murray, M.M., Howle, L.E., Fish, F.E. *Leading-edge tubercles delay stall on Humpback whale (Megaptera Novaeangliae) Flippers*, Physics of Fluids, Vol. 16, No. 5, pp. 39-42, 2004.

Skillen, A.; Revell, A.; Pinelli, A.; Piomelli, U.; Javier, J. *Flow over a wing with leading-edge undulations*. *AIAA Journal*, v. 53, n. 2, p. 464-472, 2014.

Spaho, KOSTIKA. *Biomimicry: Architecture that Imitates Nature's Functions, Forms and Parts*. Architecture Theses. Paper 72. 2011.

7. RESPONSIBILITY NOTICE

The authors Guilherme Pimentel and Heidi Korzenowski are the only responsible for the printed material included in this paper.